Structure of a hydrophobic leucinostatin derivative determined by host lattice display

Cedric Kiss[1], Flavio M. Gall[2#], Birgit Dreier[1], Michael Adams[3], Rainer Riedl[2], Andreas Plückthun[1*] and Peer R. E. Mittl[1*]

Affiliation:

[1]Department of Biochemistry, University of Zürich, Winterthurerstrasse 190, 8057 Zürich, Switzerland

[2]Institute of Chemistry and Biotechnology, Center of Organic and Medicinal Chemistry, ZHAW Zurich University of Applied Sciences, Einsiedlerstrasse 31, 8820 Wädenswil, Switzerland

[3]Bacoba AG, Elisabethenstrasse 15, 4051 Basel, Switzerland.

Current address:

[#] Welmedis GmbH, Schönenbergstrasse 12, 8820 Wädenswil, Switzerland

Corresponding author:

* Correspondence to:

Peer Mittl, phone: +41-44-635 6559, Email: mittl@bioc.uzh.ch

or

Andreas Plückthun, phone: +41-44-635 5570, Email: plueckthun@bioc.uzh.ch

Manuscript:

16 pages, 2 table, 4 figures

Supplementary material: 2 methods, 6 figures

Coordinates and structure factors have been deposited at the PDB with accession codes 8A1A and 8A1A.

Keywords:

crystal engineering, host lattice display, leucinostatin,

Abbreviations:

CCDC: Cambridge Crystallographic Data Centre

Abstract (115 words):

Peptides comprising many hydrophobic amino acids are almost insoluble under physiological buffer conditions, which complicates their structural analysis. To investigate the three-dimensional structure of the hydrophobic leucinostatin derivative ZHAWOC6027 we applied the host-lattice display technology previously developed. Two Designed Ankyrin Repeat Proteins (DARPins), recognizing a biotinylated ZHAWOC6027 derivative, have been selected from a diverse library by ribosome display under aqueous buffer conditions. ZHAWOC6027 was immobilized by means of the DARPin in the host lattice and the complex structure was determined by X-ray diffraction. ZHAWOC6027 adopts a distorted α-helical conformation. The comparison with structures of related compounds that have been determined in organic solvents reveals an elevated flexibility of the termini, which might be functionally important.

Synopsis:

Host lattice display facilitated the crystallographic analysis of a hydrophobic peptide under aqueous conditions.

1. Introduction

Leucinostatins represent a family of lipopeptides that where originally isolated from the culture broth of fungi, and identified because of their cytotoxicity to HeLa cells and bacteria. The first such lipopeptide, which was later shown to be a mixture of several compounds, was described in 1973 as "leucinostatin", because its main component was leucine (Arai *et al.*, 1973). In early studies using mass spectrometry and NMR it was shown that leucinostatin comprised a central 9-mer peptide, where the N- and C-termini were blocked by amide bonds with a short unsaturated fatty acid and an alkyldiamine, respectively (Mori *et al.*, 1983). The central 9-mer peptide is composed of leucine and non-proteinogenic amino acids, such as β-hydroxyleucine (HyLeu), β-alanine (βAla), α-aminoisobutyric acid (Aib), 4-methyl-L-proline (MePro), and (2S,4S,6S)-2-amino-6-hydroxy-4-methyl-8-oxodecanoic acid (AHMOD). The initially reported leucinostatin was a mixture of leucinostatin A and -B, which differ in the composition of the C-terminal alkyldiamine (Figure 1A). Just recently the sequence of leucinostatin A was confirmed by total chemical synthesis (Watanabe *et al.*, 2021). In nature, leucinostatins have been isolated from the fungi *Paecilomyces marquandii*, *Penicillium lilacinum*, and *Acremonium* sp. (Arai *et al.*, 1973, Radics *et al.*, 1987, Strobel *et al.*, 1997). Biosynthesis of leucinostatins in *P. lilacinum* and *Tolypocladium ophioglossoides* requires the concerted action of 20 gene products, including the non-ribosomal peptide synthetase LcsA (Wang *et al.*, 2016).

Leucinostatins A and B belong to the most toxic mycotoxins in rodents with potencies similar to the well-known aflatoxins. The minimal concentration of leucinostatins A and -B for the inhibition of proliferation of pathogenic microorganisms is in the range between 1 µg/ml and 100 µg/ml and some pathogens, such as *Plasmodium falciparum* and *Trypanosoma brucei*, are particularly susceptible. The oral LD_{50} dose in mice for leucinostatin A and -B is 5.4 mg/kg and 6.3 mg/kg, respectively (Fukushima *et al.*, 1983, Otoguro *et al.*, 2003). The cytotoxicity of leucinostatin A and -B is attributed to their ability to inhibit ATP synthesis in mitochondria as well as different phosphorylation pathways (Fukushima *et al.*, 1983). At concentrations below 300 nM, leucinostatin A and -B have been reported to inhibit the phosphoryl transfer by binding to the F_o subunit of ATPase from rat liver mitochondria (Shima *et al.*, 1990). Alanine scanning and truncation studies revealed that the central 9-mer peptide and particularly the hydroxyleucine and the second N-terminal leucine are crucial for the cytotoxic activity (Abe *et al.*, 2018). A comprehensive structure-activity study using *T. brucei* as a model organism revealed that the destabilization of the inner mitochondrial membrane, which explains the anti-protozoal activity, can also be obtained with the simplified compound ZHAWOC6027 (Brand *et al.*, 2021) (Figure 1B).

The crystal structure of the leucinostatin-related peptide helioferin A (Figure 1C) has been determined and refined at 0.9 Å resolution (Gessmann *et al.*, 2018). The helioferin A crystals were obtained from mixtures of ethanol and acetonitrile. Since we were interested in the structure of the leucinostatin derivative ZHAWOC6027 under aqueous conditions we avoided crystallization from organic solvents. Instead, we applied the recently established host-lattice display method (Ernst *et al.*, 2019). Briefly, we selected Designed Ankyrin Repeat Proteins (DARPins) against biotinylated ZHAWOC6027 under physiological conditions and fused those DARPins to the C-terminus of the crystallization scaffold Endo-α-N-acetylgalactosaminidase from *Bifidobacterium longum* (EngBF). The EngBF-DARPin:ZHAWOC6027 complex was subsequently crystallized under the established conditions for EngBF and the ZHAWOC6027 structure was determined by difference Fourier methods.

2. Materials and Methods

2.1. Synthesis of biotinylated ZHAWOC6027

For the selection of DARPins a biotinylated derivative of ZHAWOC6027 was prepared by microwave assisted solid phase peptide synthesis (Supplementary Method 1). Solid phase synthesis started at the C-terminus of the 9-mer peptide with the Fmoc-β-Ala Wang resin and progressed towards the N-terminus using the Fmoc solid phase technique as described in ref. (Brand *et al.*, 2021). In order to attach the biotin moiety on the peptide the N-terminal p-fluoro-benzoic acid from ZHAWOC6027 was replaced by a 4-aminomethylbenzoic acid, which offers an amine group for the coupling with the PEGylated biotin moiety. Finally, the biotinylated peptide was cleaved from the resin and the free carboxylic acid was amidated with 1-((dimethylamino)methyl) cyclobutan-1-amine (Acba) (Supplementary Figure 1). The structural identity of the biotinylated peptide (ZHAWOC8403) was confirmed by mass spectrometry and ^{1}H-NMR.

2.2 Selection of DARPins against ZHAWOC6027

DARPins recognizing biotinylated ZHAWOC6027 were generated by immobilizing ZHAWOC8403 alternating on MyOne T1 streptavidin-coated beads (Thermo Fisher Scientific) and Sera-Mag neutravidin-coated beads (Cytiva). Ribosome display selection of DARPins was performed essentially as described in refs. (Dreier & Plückthun, 2012, Plückthun, 2012, 2015) using a semi-automated KingFisher Flex MTP96 well platform. In order to enrich binders with high affinity, selections were performed over three rounds with decreasing amounts of immobilized ZHAWOC8403 (250, 125, and 5 pmol) and off-rate selection during the third

round, using non-biotinylated ZHAWOC6027 as competitor in a thousandfold excess. This was followed by a final recovery round (50 pmol immobilized ZHAWOC8403) without competitor. During rounds 1 to 4, plates were washed five times with WBT buffer (150 mM sodium chloride, 50 mM Tris/acetate, 50 mM magnesium acetate, 0.05% Tween-20, pH 7.5) for 2 minutes, 5 minutes, 20 minutes, and 15 minutes. The enriched DNA pool was cloned into a bacterial pQIq-based expression vector that allows the expression of the binders with an N-terminal $MRGSH_6$- and a C-terminal FLAG tag. After transformation of *E. coli* XL1-blue cells (Stratagene), 190 single DARPin clones were expressed in MTP96 well plates and lysed directly using B-PER cell lysis buffer containing freshly added lysozyme and nuclease (Thermo Fisher Scientific).

The crude bacterial cell extract of single DARPin clones was subsequently used in a high-throughput ELISA screen where the binding of the DARPin was compared in the presence and absence of the target peptide. Briefly, ZHAWOC8403 was immobilized on a neutravidin-coated MTP384 plate. Binding was analyzed using a mouse monoclonal anti-FLAG-M2 antibody (Sigma, F3165) and a goat-anti-mouse antibody coupled to alkaline phosphatase as secondary antibody (Sigma, A3562). Target-specific binding of DARPins was analyzed by following the hydrolysis of para-nitrophenylphosphate at 405 nm in an ELISA-plate reader (BioTec).

Successful binders were sequenced and the DARPins were obtained by small scale expression in MTP96 deep-well plates and purified over a MTP96-well IMAC column (HisPurTM Cobalt plates, Thermo Scientific). The composition of the final elution buffer was 300 mM sodium chloride, 50 mM sodium phosphate, 250 mM imidazole, pH 7.4. From the initial 32 hits 25 single clones were successfully sequenced and purified. To assess the aggregation behavior IMAC-purified DARPins, normalized to a concentration of 10 µM, were analyzed on a Superdex 75 5/150 gel-filtration column (GE Healthcare) connected to an Äkta Micro system (GE Healthcare) using PBS as running buffer. Chromatograms were recorded by following the absorption at 280 nm wavelength. The molecular weight was estimated using β-amylase (200 kDa), bovine serum albumin (66 kDa), carbonic anhydrase (29 kDa) and cytochrome c (12.4 kDa) as molecular mass standards. Finally, two anti- ZHAWOC6027 DARPins, designated 1016-2502-E4 and 1016-2502-F11 (abbreviated as E4 and F11 in the following sections), were identified.

2.3 Cloning of EngBF DARPin fusion proteins

DARPins_E4 and F11 were cloned into the plasmid pQIq_sfGFP_EngBF_L1_DARPin_G10_His (Ernst *et al.*, 2019), which is a derivative of the pQIq vector (a $lacI^q$ encoding derivative of pQE30 (Qiagen, Hilden, Germany)) with N-terminal sfGFP- and C-terminal His_6-tags. Both tags are fused to the EngBF construct via HRV-C3-protease cleavage sites. However, E4 and F11 belong to the N2C DARPin lineage with two internal repeats, whereas DARPin_G10 comprises three internal repeats. The amino acid sequences of DARPin_E4 and F11 were grafted into the G10 sequence and back-translated to DNA. The DNA with the grafted sequence was synthesized at Twist Biosciences (San Francisco, USA) with *HindIII/BglII* restriction sites to allow in-frame fusion with the EngBF_L1 and His_6-tag sequences.

2.4. Expression and purification of EngBF-DARPin fusion proteins

sfGFP-3C-EngBF-DARPin-3C-His_6 constructs were expressed as described in ref. (Ernst *et al.*, 2019). Briefly, *E. coli* BL21 Gold competent cells were transformed with the plasmids (Agilent), plated on agar plates, and single colonies were grown in 5 ml 2×YT medium (supplemented with 100 µg/ml ampicillin and 1% glucose) overnight at 37°C (orbital shaking at 240 rpm). For expression, 200 mL TB medium (supplemented with 100 µg/ml ampicillin and 1% glucose) was inoculated with the over-night culture and incubated at 37°C with constant agitation (190 rpm, 25 mm rotor radius) until the OD_{600} reached 0.1. The expression temperature was reduced to 25°C for 30 minutes prior to induction with IPTG at a final concentration of 0.5 mM (OD_{600} between 0.6 and 0.8). The expression temperature of 25°C and shaking in 500 mL baffled flasks was maintained for 14 hours. Cells were harvested by centrifugation for 10 minutes at room temperature (5000 *g*). The pellet was resuspended in lysis buffer (200 mM sodium chloride, 20 mM sodium phosphate, 20 mM imidazole, Pefabloc SC protease inhibitor cocktail, pH 6.3) and sonicated three times for 25 seconds on ice (Branson Ultrasonics). Cell debris were removed by centrifugation (20 minutes, 20000 *g*, 25°C). Protein purification was then done at room temperature with buffers precooled to 4 °C. The supernatant was loaded on a Ni-NTA column (Quiagen, 5 mL). The column was washed with 9 column volumes (CV) wash buffer (200 mM sodium chloride, 20 mM sodium phosphate, 20 mM imidazole, 10% (v/v) glycerol, pH 6.3), 9 CV low salt washing buffer (20 mM sodium chloride, 20 mM sodium phosphate, 20 mM imidazole, 10% (v/v) glycerol, pH 6.3), 9 CV high salt washing buffer (1 M sodium chloride, 20 mM sodium phosphate, 20 mM imidazole, 10% (v/v) glycerol, pH 6.3), and finally with 9 CV wash buffer. The protein was eluted with 4.5 CV

elution buffer (200 mM sodium chloride, 20 mM sodium phosphate, 250 mM imidazole, 10% (v/v) glycerol, pH 6.3).

The eluate was directly loaded on a DARPin_R7 affinity column that specifically recognizes the N-terminal sfGFP-tag (DARPin_R7 coupled to Sepharose, 3 mL, Supplementary Methods 2). (Hansen *et al.*, 2017) The resin was washed with 15 CV wash buffer containing 200 mM sodium chloride, 15 CV wash buffer containing 20 mM sodium chloride, 15 CV wash buffer containing 1 M sodium chloride, and finally with 15 CV crystallization buffer (200 mM sodium chloride, 20 mM sodium phosphate, pH 6.3). The EngBF-DARPin fusion protein was eluted in batch mode: after adding 2 ml crystallization buffer containing 1 mg HRV-C3-protease the mixture was incubated 3 hours at room temperature with gentle agitation. The resin was washed with 10 mL crystallization buffer. The supernatant and the washing solution were combined and applied to a Ni-NTA column (Qiagen, 2 mL) to remove the cleaved His_6-tag. Purified proteins were directly used for crystallization

2.5. Characterization by surface plasmon resonance

Affinities were measured by surface plasmon resonance on a ProteOn XPR36 instrument equipped with a Neutravidin-containing NLC chip (Bio-Rad) in PBS supplemented with 0.005% Tween-20. Two ligand channels were coated with 30 nM ZHAWOC8403 for 170 seconds (70 response units). Unfused DARPins or EngBF-DARPin fusions were injected at flow rates of 60 µl/min for 360 seconds followed by a dissociation phase of 1800 seconds. In between measurements the chip was regenerated with 1.5 mM glycine, pH 2.5. Data were processed using ProteOn™ Manager software (version 3.1.0.6). The processed sensogram data were imported in the BIAevaluation software (version 4.1) and fitted with different kinetic titration models.

2.6. Structure determination

EngBF_L1_DARPin fusion proteins were concentrated to 10-20 mg/ml using Amicon Ultra-4 centrifugal concentrators (50 kDa MW cut-off, Merck Millipore). A 10 mM stock solution of ZHAWOC6027 was prepared in DMSO. 50 µL protein solution was mixed with 15 µL ZHAWOC6027 stock solution (approximately 20 to 40-fold molar excess) and incubated on ice for 1 hour. The protein:peptide mixture was set up for crystallization in sitting-drop vapor-diffusion experiments in 96-well plates. Crystallization conditions were screened around the established conditions for EngBF crystals (25% 2-methyl-2,4-pentanediol (MPD), 3% PEG 20000, 0.2 M sodium chloride, 0.01 M manganese chloride, 0.1 M MES, pH 6.9) (Suzuki *et al.*, 2009), changing the pH along the columns (from pH 6 to 7) and the MPD/PEG 20,000 ratio

along the rows (MPD from 23% to 27% (v/v) and PEG 20,000 from 5% to 2% (w/v)). Three different ratios of reservoir- to protein solution (1:1, 2:1, 3:1) in 300–400 nL drops were used per well and incubated against 75 µL of reservoir solution at 4 °C. Crystals of constructs EngBF_L1_E4_v1, EngBF_L1_E4_v2, and EngBF_L1_F11_v1 grew within 25 days, whereas construct EngBF_L1_F11_v2 did not crystallize under the expected conditions.

Crystals were mounted in cryo-loops from Hampton Research and flash-cooled in liquid nitrogen without any further cryo-protectant. X-ray diffraction data were collected at a wavelength of 1.0 Å on beamline X06SA (Swiss Light Source, Paul Scherrer Institute, Villigen, Switzerland) equipped with an Eiger 16M detector (Dectris, Baden-Wättwil, Switzerland). Data were processed with XDS, Aimless, and autoPROC (Evans, 2011, Kabsch, 2010, Vonrhein *et al.*, 2011). To ensure unique assignment of the polar 6_5-screw axis and consistent allocation of test reflections, we used the EngBF_L1_G10 diffraction data as a reference dataset (PDB ID: 6QFK) (Ernst *et al.*, 2019). The calculation of electron density and refinement was done using BUSTER version 2.10.4. The difference electron density was sharpened using the ligand chasing option (-L) in BUSTER. Restraints for the ZHAWOC6027 peptide were calculated using the GRADE server (Smart *et al.*, 2011). After an initial refinement round without peptide the difference electron density was sufficiently clear to position the ZHAWOC6027 molecule using the program Rhofit (Smart *et al.*, 2014). Refinement statistics are given in Table 2. For model building and preparation of figures we used Coot and Pymol (DeLano, 2002, Emsley *et al.*, 2010). Structures were deposited at the PDB with the accession numbers given in Table 2. Raw diffraction data were uploaded to www.proteindiffraction.org.

3. Results

In order to display the target molecule ZHAWOC6027 in a unique orientation in the host lattice a selectively binding DARPin is required. Typically, targets for the selection of DARPins by ribosome display are immobilized using the tight interaction between biotin and neutravidin. A biotin moiety was therefore coupled to the N-terminal benzoyl group of ZHAWOC6027 via an amide bond. The biotinylated compound ZHAWOC8403 harbors an 11-mer polyethylene glycol (PEG) linker to prevent steric hindrance between the peptide moiety and the nascent DARPin chain during ribosome display (Supplementary Figure 1).

ZHAWOC8403 was immobilized to select binders from a DARPin library (Plückthun, 2012, Brauchle *et al.*, 2014, Schilling *et al.*, 2014, Plückthun, 2015) that encodes DARPins with 3 internal repeats (N3C) and a stabilized C-cap with and without randomized capping repeats (Kramer *et al.*, 2010). Initially 32 clones were sequenced and 25 unique DARPins were

identified. Just 2 out of 25 isolated hits belonged to the N3C lineage, whereas the remaining 23 hits contained only 2 internal repeats (N2C), which are present in small quantities due to the assembly process of the library from single repeat building blocks. Finally, only two hits, designated E4 and F11, showed a clear signal in the high-throughput ELISA screen (Supplementary Figure 2). DARPin E4 shows a higher signal compared to F11 and it is clearly monomeric, which is not the case for F11 (data not shown).

DARPins E4 and F11 were fused to the C-terminus of EngBF using the rigid-helix fusion strategy (Wu *et al.*, 2017, Batyuk *et al.*, 2016). Two different fusion strategies, designated L1 and L2, were previously developed (Ernst *et al.*, 2019). Since ZHAWOC6027 is a relatively small target we used the L1 design, because L1 possesses lower B-factors for the DARPin domain at the expense of less space for the target compared to L2. In both designs, an N3C DARPin is required to bridge the gap between symmetry-related molecules in the EngBF crystal lattice. Therefore, the N2C DARPin E4 and F11 sequences were grafted onto the EngBF_L1_G10 design, which is an N3C DARPin. Due to the repetitive architecture of DARPins two alternative alignment registers between the N2C DARPins E4 (or F11) and the N3C DARPin G10 are meaningful (constructs v1 and v2). Two fusion constructs between EngBF and DARPin E4 in the alignment registers v1 or v2 were thus generated by transferring residues at the randomized positions from E4 to EngBF_L1_G10 depending on the selected alignment register. Since side chains from the N- and C-caps can participate in target binding and were randomized in the DARPin library, some residues from the caps that are lining the DARPin paratope were transferred as well. For DARpin F11 we applied the same strategy (Figure 2).

All four EngBF-DARPin fusion proteins were expressed in *E. coli* BL21 Gold cells. The purified constructs were analyzed by SPR (Table 1). The SPR analysis confirmed the observations made in the initial ELISA screen, namely that unfused DARPin E4 binds ZHAWOC8403 significantly better than DARPin F11. For DARPin E4 the alignment register v1 was superior over the alignment register v2, because EngBF_L1_E4_v1 binds ZHAWOC8403 with similar kinetic constants like unfused DARPin E4, whereas no binding was detected for EngBF_L1_E4_v2 (Supplementary Figure 3). For DARPin F11 it was the opposite: EngBF_L1_F11_v1 shows equally poor binding characteristics like DARPin F11, whereas alignment register v2 showed a clearly improved binding for EngBF_L1_F11_v2.

Crystallization of all four EngBF-DARPin fusions in complex with ZHAWOC6027 was tested under the established conditions of EngBF (Ernst *et al.*, 2019). All fusions except EngBF_L1_F11_v2 crystallized at very similar MPD concentrations and in the same pH range.

No attempts were made to establish new crystallization conditions for EngBF_L1_F11_v2. Crystals of EngBF_L1_E4_v1, EngBF_L1_E4_v2, and EngBF_L1_F11_v1 in complex with ZHAWOC6027 were analyzed at the SLS beamline X06SA and diffracted to 2.36 Å, 2.08 Å, and 2.05 Å resolution, respectively. Difference Fourier analysis between the observed diffraction data and the isomorphic EngBF_L1_G10 structure (PDB ID: 6QFK) (Ernst *et al.*, 2019) without bound peptide showed clear difference electron density for ZHAWOC6027 at the expected position in EngBF_L1_E4_v1, weaker density in EngBF_L1_F11_v1 and no density in EngBF_L1_E4_v2 (Figure 3A to C). Therefore, refinement of the EngBF_L1_E4_v2 structure was abandoned. Initially, the peptide was fitted into the weaker difference electron density of EngBF_L1_F11_v1. The conformation of the peptide was confirmed later when the EngBF_L1_E4_v1:ZHAWOC6027 data became available. For EngBF_L1_E4_v1:ZHAWOC6027 all residues from the peptide except the C-terminal βAla9 and Acba are resolved in the final electron density map, whereas EngBF_L1_F11_v1:ZHAWOC6027 shows only density for residues CyHex2 to Leu6 (Figure 3D and E). The poor density is probably a consequence of the B-factor gradient of the host lattice (Supplementary Figure 4A and B). The average B-factor for the DARPin domain is approximately two times that of the EngBF domain, and the ZHAWOC6027 B-factor is even higher than the DARPin B-factor (Table 2).

In the EngBF_L1_E4_v1:ZHAWOC6027 complex, peptide residues CyHex2 to Aib8 adopt a distorted α-helical conformation with canonical H-bonds between Leu3-O···Aib7-N (2.9 Å), Aib4-O···Aib8-N (3.5 Å), and Leu5-O···βAla9-N (3.5 Å). The distance between CyHex2-O and Leu6-N (4.2 Å) is too long for a H-bond. Despite the weak electron density this conformation is also seen in the EngBF_L1_F11_v1 complex (Figure 4A). ZHAWOC6027 binds to EngBF_L1_E4_v1 in a parallel orientation. Upon binding a surface area of 612 $Å^2$ is buried at the interface, accounting for 46% of the ZHAWOC6027 molecular surface (Supplementary Figure 4C). The E4 paratope is dominated by hydrophobic amino acids, because ZHAWOC6027 comprises only hydrophobic residues as well. However, the ZHAWOC6027 main chain participates in H-bonds, e.g. the ZHAWOC6027 helix dipole moment is compensated by polar residues from EngBF_L1_E4_v1. The Gln1559 and Arg1634 side chains form H-bonds with the ZHAWOC6027 N- and C-termini, respectively (Gln1559-NE2···Pro1-O, 3.1 Å; Gln1559-OE1···Leu3-N, 3.0 Å; Arg1634-NH2···Leu6-O, 3.6 Å; Arg1634-NE···Aib7-O, 3.0 Å) (Figure 4B). Furthermore, the ZHAWOC6027 main chain interacts via water-mediated H-bonds with the Asp1621 side chain (Asp1621-OD2···Wat914···Wat915···Aib4-O). The side chains of residues Pro1, CyHex2, Leu5 and

Leu6 from ZHAWOC6027 are exposed to the solvent, but Leu3, Aib4, Aib7 and Aib8 interact with Leu1564, Phe1567, Thr1590, Thr1592, Leu1597, Ala1600, and Leu1630 side chains from EngBF_L1_E4_v1 (Figure 4C). Even though CyHex2 is partially solvent exposed it forms hydrophobic contacts with the Tyr1557 and Val1589 side chains and the Fben group at the N-terminus of ZHAWOC6027 rests against the Trp1534 side chain. ZHAWOC6027 is recognized mainly by residues from the 1st and 2nd internal repeat of EngBF_L1_E4_v1, which have been grafted from the parental DARPin E4 in the v1 alignment register (Supplementary Figure 4B and Figure 2). Only Asp1621, Leu1630, and Arg1634 belong to the 3rd internal repeat. Asp1621 and Leu1630 are invariant in the DARPin framework and Arg1634 was grafted from the DARPin E4 C-cap.

Bound ZHAWOC6027 shows a similar structure like leucinostatin A (CCDC entry: 1183178) (Cerrini *et al.*, 1989) and helioferin A (PDB ID: 6EVH) (Gessmann *et al.*, 2018), which have been obtained by crystallizing the free peptides from organic solvents. Particularly residues Leu3 to Aib8 adopt the same α-helical conformation in all three structures (Figure 4D). Differences exist at the termini, however: at the N-terminus of ZHAWOC6027 CyHex2 has rotated by approximately 180° around the CyHex2 Cα-C bond. We tried to model ZHAWOC6027 in the conformation seen in leucinostatin A, but placing the bulky Fben-Pro1 moiety into the CyHex2 side chain density causes strong difference electron density around CyHex2, suggesting that the current assignment is correct. At the C-terminus of leucinostatin A, βAla9 and DPDA adopt a 3.10-helix conformation, whereas in EngBF_L1_E4_v1:ZHAWOC6027, βAla9 and Acba are disordered, probably because the Arg1634 side chain from EngBF_L1_E4_v1 occupies the βAla9 position.

4. Discussion

Crystal structures of isolated hydrophobic peptides like leucinostatin A and helioferin A revealed completely helical conformations with 7 canonical H-bonds involving all residues from the peptides. For ZHAWOC6027 a similar three-dimensional structure was assigned based on NOE-NMR data recorded in deuterated methanol (Brand *et al.*, 2021). But what kind of structure does a poorly soluble hydrophobic peptide like ZHAWOC6027 adopt under aqueous conditions? To answer this question we applied the host-lattice display technology to ZHAWOC6027 (Ernst *et al.*, 2019). We selected two DARPins that recognize ZHAWOC6027 with high affinity, and thus at low concentration in PBS. The DARPin library encodes predominantly DARPins with three internal repeats. However, DARPins with just two internal repeats were selected, because shorter variants are preferred during the PCR amplification step

and in the present case, the third internal repeat does not improve the affinity for ZHAWOC6027 to compensate for this disadvantage.

DARPin E4 binds ZHAWOC6027 with nanomolar affinity, but the SPR data does not follow the expected 1:1-binding model (Table 1). Instead, either a heterogenous ligand- or a two-step binding model (data not shown) were required to interpret the sensorgram data (Supplementary Figure 3). Considering the flexibility of the N- and C-termini of ZHAWOC6027 (Figure 4A), a binding model where the immobilized ligand adopts different conformations is conceivable and has been observed previously for other short antimicrobial peptides, such as melittin (Hall & Aguilar, 2010).

Interestingly, grafting of N2C DARPin E4 on the N3C EngBF_L1_G10 was only successful in one of the two registers. The EngBF_L1_E4_v1 fusion protein shows similar k_{off} rates compared to unfused DARPin E4, whereas the k_{on} rates are one order of magnitude slower (Table 1). Since k_{on} depends on the diffusion coefficient of the analyte a slower k_{on} rate for the significantly larger EngBF fusion protein was expected. Unexpectedly, the alignment register v2 abrogated binding completely. Hence, no difference electron density for the ligand was observed (Figure 3C). The lack of affinity could be caused by steric clashes between the ligand and the EngBF_L1 framework residues in the v2 register. The EngBF_L1_E4_v1:ZHAWOC6027 structure reveals that the N-terminal fluorobenzoyl group would bind close to the N-terminus of the parental DARPin E4 (Supplementary Figure 5). In the v1 register, there is sufficient space for the fluorobenzoyl group, because the N-terminal helix is straight, but in the v2 register the fluorobenozyl group would clash with the Glu1559 side chain from the preceding framework repeat.

DARPin F11 shows a lower affinity for ZHAWOC6027 compared to E4, which was already seen in the initial high-throughput ELISA and later confirmed by SPR (Supplementary Figures 2 and 3, Table 1). Grafting of F11 in the alignment register v1 decreased the affinity even further. The weak difference electron density in EngBF_L1_F11_v1 thus comes without surprise, considering a lower occupancy due to the poorer binding affinity. Interestingly, the alternative v2 register significantly improved the affinity, but the complex no longer crystallizes under the established conditions. Both observations support the hypothesis that grafting of F11 in the alignment register v2 could have altered the overall structure of the DARPin. Even a gentle bending of the DARPin superhelix would prevent EngBF_L1_F11_v2 from adopting the expected crystal lattice and it could open up the DARPin paratope with the consequence of a superior binding affinity.

ZHAWOC6027 shows similar conformations in EngBF_L1_E4_v1 and EngBF_L1_F11_v1 (Figure 4A) because both DARPins possess similar residues at the randomized positions (Figure 2) and many hydrophobic residues are even identical as shown in Figure 4C. Differences occur at the ZHAWOC6027 termini. Gln1559 and Arg1634 from E4, which recognize the N- and C-termini of ZHAWOC6027, respectively, are replaced by Thr1559 and Trp1634 in F11. Additionally, E4 residues Thr1590 and Thr1592, which contact the hydrophobic Aib4 from ZHAWOC6027, are replaced by Leu1590 and Asp1592 in F11. Surprisingly, hydrophilic residues, such as Thr and Asp, occur at position 1592, despite the hydrophobicity of the ligand. In both cases the side chain at position 1592 forms H-bonds, either with Thr1590 in E4 or with the framework residue Asp1621 in F11.

Both structures confirm that ZHAWOC6027, and perhaps other leucinostatin derivatives as well, can adopt conformations which are less compact than the chiefly α-helical conformations seen in crystal structures of free leucinostatin A and helioferin or the NMR structure of free ZHAWOC6027 (Cerrini *et al.*, 1989, Gessmann *et al.*, 2018, Brand *et al.*, 2021). The free structures have been obtained from highly concentrated samples analyzed in organic solvents, which support the formation of intramolecular H-bonds. The complex structures presented above suggest that the ZHAWOC6027 termini are flexible under aqueous conditions. The common feature of the free and complexed structures is the α-helical conformation of Leu3 to Aib8 (Figure 4D). This fragment contains three Aib residues. Due to the bulky methyl group that replaces the Cα proton in alanine, Aib is a stronger inducer of 3.10- and α-helices than any other proteinogenic amino acid (Schweitzer-Stenner *et al.*, 2007). Particularly the N-terminus shows a transition from a α-helical conformation with an (n to n+4) H-bond pattern towards a 3.10-helix with an (n to n+3) H-bond pattern, because the distance between CyHex2-O and Leu5-N (4.1 Å) is shorter than the distance between CyHex2-O and Leu6-N (4.2 Å). Similar structural transitions from 3.10- to α-helical conformations are seen in other Aib-rich peptides, such as efrapeptidin (Supplentary Figure 6).

The structural mobility of the ZHAWOC6027 N-terminus might be functionally important, because it was shown that particularly the N-terminal residues HyLeu3 and Leu5 are crucial for the anti-proliferative activity of leucinostatin derivatives in cellular assays (Abe *et al.*, 2018). Unfortunately, the molecular target for the cytotoxic activity of leucinostatin A is not known precisely. It was suggested that leucinostatin A and certain derivatives may either act as ionophores of the inner mitochondrial membrane (Brand *et al.*, 2021, Csermely *et al.*, 1994, Fresta *et al.*, 2000) or target the F_1F_0-ATP synthase (Shima *et al.*, 1990). Perhaps, the structural flexibility of ZHAWOC6027 seen in the EngBF_L1_E4_v1 construct resembles the structural

adaptation of ZHAWOC6027 to a complex binding site that requires a partial restructuring of the α-helix conformation. Provided that ZHAWOC6027 is flexible at the termini in aqueous solution, binding to the DARPin paratope will also have an impact on its conformation. However, the selection of a suitable binder can only be successful to a conformation that is sufficiently populated and remains present in the aliquots that are used on different days over the different selection rounds. Under these conditions, DARPins can be picked from the library that are compatible with a defined solution structure of ZHAWOC6027. If ZHAWOC6027 were intrinsically unstructured and disordered in aqueous solution, we would expect that the free and complexed structures are substantially different from each other. Since this is not the case we assume that ZHAWOC6027 possesses a rather stable helical conformation with elevated flexibility of the termini under aqueous conditions.

Acknowledgements

We would like to thank the following persons for skillful technical support: Thomas Reinberg and Sven Furler from the high-throughput DARPin selection platform, Tong Chen and Loan Nguyen for cloning and sequencing, Gabriela Nagy-Davidescu for SPR experiments, Jens Sobek from the Functional Genomics Center Zürich for discussing the SPR analysis, Beat Blattmann from the high-throughput crystallization center at the University of Zürich, and the staff from beamlines X06SA and X06DA at the Swiss Light Source (PSI, Villigen, Switzerland) for supporting diffraction data collection.

Funding information

This project was supported by grant F-41105-23-01 from the *Stiftung für wissenschaftliche Forschung*, University Zürich to P.R.E.M, and by grant CTI 19208.1 PFLS-LS from the *Swiss Commission for Technology and Innovation* as well as direct financial contributions from *Bacoba AG, Basel* to R.R.

Conflict of interest

M. Adams is currently CEO of Bacoba AG, who supported this research financially, and logistically.

References

Abe, H., Kawada, M., Sakashita, C., Watanabe, T. & Shibasaki, M. (2018). *Tetrahedron* **74**, 5129-5137.

Abrahams, J. P., Buchanan, S. K., Van Raaij, M. J., Fearnley, I. M., Leslie, A. G. & Walker, J. E. (1996). *Proc Natl Acad Sci U S A* **93**, 9420-9424.

Arai, T., Mikami, Y., Fukushima, K., Utsumi, T. & Yazawa, K. (1973). *J Antibiot (Tokyo)* **26**, 157-161.

Batyuk, A., Wu, Y., Honegger, A., Heberling, M. M. & Plückthun, A. (2016). *J Mol Biol* **428**, 1574-1588.

Brand, M., Wang, L., Agnello, S., Gazzola, S., Gall, F. M., Raguz, L., Kaiser, M., Schmidt, R. S., Ritschl, A., Jelk, J., Hemphill, A., Maser, P., Butikofer, P., Adams, M. & Riedl, R. (2021). *Angew Chem Int Edit* **60**, 15613-15621.

Brauchle, M., Hansen, S., Caussinus, E., Lenard, A., Ochoa-Espinosa, A., Scholz, O., Sprecher, S. G., Plückthun, A. & Affolter, M. (2014). *Biol Open* **3**, 1252-1261.

Cerrini, S., Lamba, D., Scatturin, A. & Ughetto, G. (1989). *Biopolymers* **28**, 409-420.

Csermely, P., Radics, L., Rossi, C., Szamel, M., Ricci, M., Mihaly, K. & Somogyi, J. (1994). *Biochim Biophys Acta* **1221**, 125-132.

DeLano, W. L. (2002). *The PyMOL Molecular Graphics System.*

Dreier, B. & Plückthun, A. (2012). *Methods Mol Biol* **805**, 261-286.

Emsley, P., Lohkamp, B., Scott, W. G. & Cowtan, K. (2010). *Acta Crystallogr D Biol Crystallogr* **66**, 486-501.

Ernst, P., Plückthun, A. & Mittl, P. R. E. (2019). *Sci Rep-Uk* **9**.

Evans, P. R. (2011). *Acta Crystallogr D Biol Crystallogr* **67**, 282-292.

Fresta, M., Ricci, M., Rossi, C., Furneri, P. M. & Puglisi, G. (2000). *J Colloid Interf Sci* **226**, 222-230.

Fukushima, K., Arai, T., Mori, Y., Tsuboi, M. & Suzuki, M. (1983). *J Antibiot* **36**, 1613-1630.

Gessmann, R., Bruckner, H., Berg, A. & Petratos, K. (2018). *Acta Crystallogr D* **74**, 315-320.

Hall, K. & Aguilar, M. I. (2010). *Methods Mol Biol*, 2010/03/11 ed., pp. 213-223.

Hansen, S., Stuber, J. C., Ernst, P., Koch, A., Bojar, D., Batyuk, A. & Plückthun, A. (2017). *Sci Rep* **7**, 16292.

Kabsch, W. (2010). *Acta Crystallogr D Biol Crystallogr* **66**, 125-132.

Kim, M. H., Woo, S. K., Kim, K. I., Lee, T. S., Kim, C. W., Kang, J. H., Kim, B. I., Lim, S. M., Lee, K. C. & Lee, Y. J. (2015). *ACS Med Chem Lett* **6**, 528-530.

Kramer, M. A., Wetzel, S. K., Plückthun, A., Mittl, P. R. & Grütter, M. G. (2010). *J Mol Biol* **404**, 381-391.

Mori, Y., Suzuki, M., Fukushima, K. & Arai, T. (1983). *J Antibiot (Tokyo)* **36**, 1084-1086.

Otoguro, K., Ui, H., Ishiyama, A., Arai, N., Kobayashi, M., Takahashi, Y., Masuma, R., Shiomi, K., Yamada, H. & Omura, S. (2003). *J Antibiot* **56**, 322-324.

Plückthun, A. (2012). *Methods Mol Biol* **805**, 3-28.

Plückthun, A. (2015). *Annu Rev Pharmacol Toxicol* **55**, 489-511.

Radics, L., Kajtarperedy, M., Casinovi, C. G., Rossi, C., Ricci, M. & Tuttobello, L. (1987). *J Antibiot* **40**, 714-716.

Schilling, J., Schoppe, J. & Plückthun, A. (2014). *J Mol Biol* **426**, 691-721.

Schweitzer-Stenner, R., Gonzales, W., Bourne, G. T., Feng, J. A. & Marshall, G. R. (2007). *J Am Chem Soc* **129**, 13095-13109.

Shima, A., Fukushima, K., Arai, T. & Terada, H. (1990). *Cell Struct Funct* **15**, 53-58.

Smart, O. S., Womack, T. O., Sharff, A., Flensburg, C., Keller, P., Paciorek, W., Vonrhein, C. & Bricogne, G. (2011). *Grade, version 1.2.20.*

Smart, O. S., Womack, T. O., Sharff, A., Flensburg, C., Keller, P., Paciorek, W., Vonrhein, C. & Bricogne, G. (2014). *RHOFIT, version 1.2.4.*

Strobel, G. A., Torczynski, R. & Bollon, A. (1997). *Plant Sci* **128**, 97-108.

Suzuki, R., Katayama, T., Kitaoka, M., Kumagai, H., Wakagi, T., Shoun, H., Ashida, H., Yamamoto, K. & Fushinobu, S. (2009). *J Biochem* **146**, 389-398.
Vonrhein, C., Flensburg, C., Keller, P., Sharff, A., Smart, O., Paciorek, W., Womack, T. & Bricogne, G. (2011). *Acta Crystallogr D Biol Crystallogr* **67**, 293-302.
Wang, G., Liu, Z. G., Lin, R. M., Li, E. F., Mao, Z. C., Ling, J., Yang, Y. H., Yin, W. B. & Xie, B. Y. (2016). *Plos Pathog* **12**.
Watanabe, T., Abe, H. & Shibasaki, M. (2021). *Chem Rec* **21**, 175-187.
Wu, Y., Batyuk, A., Honegger, A., Brandl, F., Mittl, P. R. E. & Plückthun, A. (2017). *Sci Rep* **7**, 11217.

Tables

Table 1. Binding kinetics for ZHAWOC8403 determined by SPR.

Construct	**Kinetic Model***	**$k_{on}1$ [$(M\ s)^{-1}$]**	**$k_{off}1$ [s^{-1}]**	**Kd1 [M]**	**$R_{max}1$**	**$k_{on}2$ [$(M\ s)^{-1}$]**	**$k_{off}2$ [s^{-1}]**	**Kd2 [M]**	**$R_{max}2$**	**$\chi 2$**
DARPin E4	HL	$1.15 \cdot 10^{5}$	$4.39 \cdot 10^{-4}$	$3.80 \cdot 10^{-9}$	29.9	$2.06 \cdot 10^{6}$	$1.09 \cdot 10^{-2}$	$5.32 \cdot 10^{-9}$	44.6	4.94
DARPin F11	L	$3.54 \cdot 10^{4}$	$9.33 \cdot 10^{-4}$	$2.64 \cdot 10^{-8}$						2.97
EngBF-L1_ DARPin_E4_v1	HL	$1.56 \cdot 10^{4}$	$4.45 \cdot 10^{-4}$	$2.87 \cdot 10^{-8}$	9.6	$7.32 \cdot 10^{4}$	$1.13 \cdot 10^{-2}$	$1.55 \cdot 10^{-7}$	16.3	2.87
EngBF-L1_ DARPin_E4_v2	no fit	n.d.	n.d.	n.d.						
EngBF-L1_ DARPin_F11_v1	LB	1.04	$9.97 \cdot 10^{-6}$	$9.61 \cdot 10^{-6}$						7.52
EngBF-L1_ DARPin_F11_v2	HL	$5.27 \cdot 10^{4}$	$4.49 \cdot 10^{-4}$	$8.54 \cdot 10^{-9}$	59.9	$7.50 \cdot 10^{4}$	$4.01 \cdot 10^{-3}$	$5.34 \cdot 10^{-8}$	73.4	1.95

n.d.: not determined

*Data were fitted using the following models: HL, heterogenous ligand, L, Langmuir 1:1 model, LB, Langmuir with baseline drift as implemented in the BIAevaluation Software

Table 2. Data collection and refinement statistics.

	EngBF_L1E4v1: ZHAWOC6027	**EngBF_L1F11v1: ZHAWOC6027**
PDB ID	**8A19**	**8A1A**
Crystallization conditions	2.55 % PEG20000, 26.72 % MPD 0.2M NaCl, 0.01M $MnCl_2$, 0.1M MES, pH 6.43	3.64 % PEG20000, 24.82 % MPD 0.2M NaCl, 0.01M $MnCl_2$, 0.1M MES, pH 6.43
Data statistics		
Resolution range (Å)*	98.94-2.36 (2.47-2.36)	166.161-2.05 (2.24-2.05)
Space group	$P6_5$	$P6_5$
Unit cell	192.76 192.76 122.83 90 90 120	191.87 191.87 122.41 90 90 120
Total reflections	1147539 (60193)	5229568 (250280)
Unique reflections	96740 (4841)	123411 (6170)
Multiplicity	11.9 (12.4)	42.4 (40.6)
Completeness (%)		
spheroidal	90.60 (35.9)	76.6 (16.2)
ellipsoidal	94.8 (51.0)	96.2 (70.8)
Mean I/sigma (I)	8.8 (1.5)	13.9 (1.7)
Wilson B-factor	42.24	38.67
ISA	20.09	23.71
R-merge#	0.227 (1.950)	0.290 (3.217)
R-meas#	0.237 (2.033)	0.294 (3.258)
R-pim#	0.069 (0.575)	0.045 (0.510)
CC1/2	0.996 (0.599)	0.998 (0.698)
Refinement statistics		
Resolution range (Å)*	34.52-2.36 (2.44-2.36)	49.28-2.05 (2.12-2.05)
Reflections used in refinement	96686 (3079)	123376 (772)
Reflections used for R-free	4853 (161)	6165 (37)
R-work	0.1550 (0.2443)	0.1539 (0.2456)
R-free	0.1831 (0.2755)	0.1761 (0.2490)
Number of atoms	11807	12109
macromolecules	10419	10435
ligands	137	136
solvent	1251	1538
Protein residues	1345	1345
RMS (bonds)	0.012	0.011
RMS (angles)	1.61	1.58
Ramachandran		
favored (%)	96.35	96.72
allowed (%)	3.57	3.13
outliers (%)	0.07	0.15
Rotamer outliers (%)	1.99	2.34
Clashscore	1.94	1.74
Average B-factor	51.85	49.81
macromolecules	50.94	48.08
..- EngBF	43.71	40.64
..- DARPin	102.97	101.49
ligands	105.27	115.38
..- ZHAWOC6027	120.79	142.49
solvent	53.55	55.75

*Statistics for the highest-resolution shell are shown in parentheses.
#calculated for all I+ and I- measurements together.

Figure legends

Figure 1. Formulas and sequences of (A) leucinostatin A (R=CH_3) and -B (R=H), (B) ZHAWOC6027, and (C) helioferin A. Structural motifs that are different from leucinostatin A are shown in red. Amino acids are numbered and abbreviated as follows: Mha, (4S,2E)-4-methylhex-2-enoic acid; MePro, 4-methyl-L-proline; AHMOD, (2S,4S,6S)-2-amino-6-hydroxy-4-methyl-8-oxodecanoic acid; HyLeu, β-hydroxyleucine; Aib, aminoisobutyric acid; βAla, 3-aminopropionic acid; DPDA, N1,N1-dimethylpropane-1,2-diamine; Fben, p-fluorobenzoic acid; CyHex, (S)-2-amino-4-cyclohexylbutanoic acid; Acba, 1-((dimethylamino)methyl)cyclobutan-1-amine; M8A, (2R)-2-methyl-n-1-octanoic acid; Apae, 2-(2'-aminopropyl) aminoethanol.

Figure 2. Grafting of DARPins E4 and -F11 on EngBF_L1_G10 using two different alignment registers (v1 and v2). Capping repeats and the EngBF framework are shown in dark and light grey, respectively. Internal repeats 1 and 3 are highlighted in yellow, and internal repeat 2 in cyan. Cys1655, which is crucial for the crystal contact, is emphasized in red. Vertical boxes indicate residues at randomized positions. EngBF residues (up to residue number 1503), which are identical in all constructs, have been omitted for clarity.

Figure 3. Electron density maps for ZHAWOC6027 bound to the DARPin paratope. The difference electron density maps without sharpening are shown in red and green at contour levels -4σ and +4σ, respectively, for (A) EngBF_L1_E4_v1, (B) EngBF_L1_F11_v1, and (C) EngBF_L1_E4_v2. The final σ_A-weighted 2Fo-Fc maps were contoured at 1σ and shown in blue for (D) EngBF_L1_E4_v1 and (E) EngBF_L1_F11_v1. Residues 1517-1680 from the EngBF-DARPin fusion are shown as a grey cartoon with the N-terminus at the top left.

Figure 4. Recognition of ZHAWOC6027 by EngBF_L1_E4_v1. H-Bonds are shown as dashed lines in grey. (A) Superposition of ZHAWOC6027 from EngBF_L1_E4_v1 (orange carbons) and EngBF_L1_F11_v1 (wheat carbons). The βAla9-Acba moiety is shown with white carbons, because it is not defined in the electron density map. Polar (B) and hydrophobic (C) interactions at the ZHAWOC6027 binding site. DARPin E4 repeats are colored like in Figure 2. Residues belonging to ZHAWOC6027 are labeled in orange. (D) Superposition of leucinostatin A (green carbons) and helioferin A (pink carbons) on ZHAWOC6027. Residues from leucinostatin A are labeled in green.

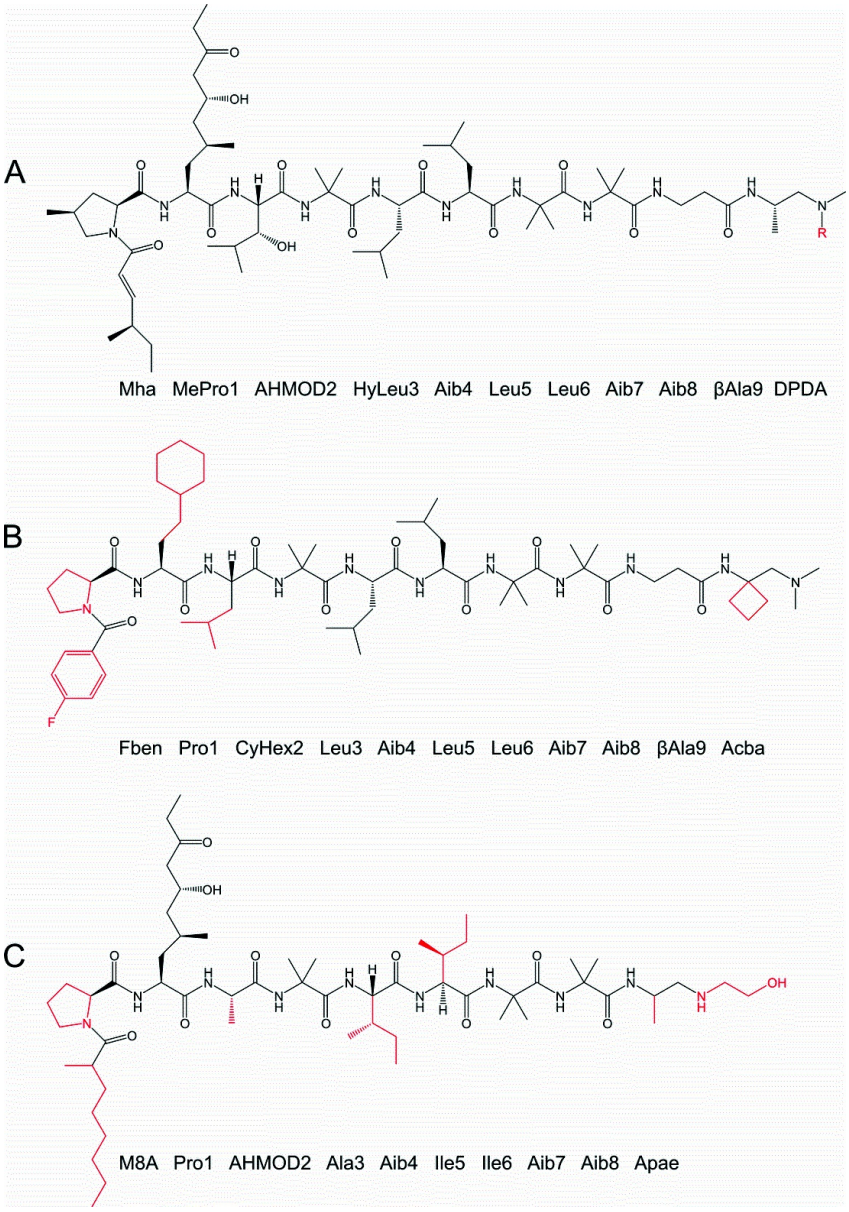
A
Mha MePro1 AHMOD2 HyLeu3 Aib4 Leu5 Leu6 Aib7 Aib8 βAla9 DPDA
B
Fben Pro1 CyHex2 Leu3 Aib4 Leu5 Leu6 Aib7 Aib8 βAla9 Acba
C
M8A Pro1 AHMOD2 Ala3 Aib4 Ile5 Ile6 Aib7 Aib8 Apae

Figure 1

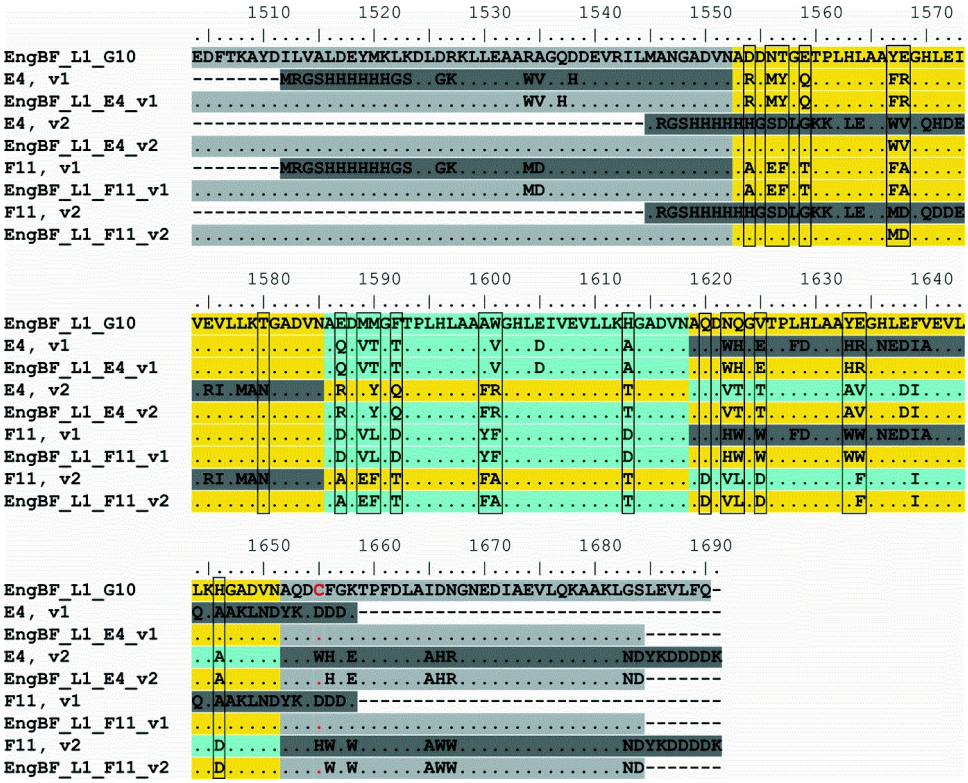
1510 1520 1530 1540 1550 1560 1570
EngBF_L1_G10 EDFTKAYDILVALDEYMKLKDLDRKLLEAARAGQDDEVRILMANGADVNADDNTGETPLHLAAYEGHLEI
E4, v1 --------MRGSHHHHHHGS..GK.....WV..H.....R.MY.Q.....FR.....
EngBF_L1_E4_v1 .....WV.H.....R.MY.Q.....FR.....
E4, v2 -----.RGSHHHHHHGSDLGKK.LE..WV.QHDE
EngBF_L1_E4_v2 .....WV.....
F11, v1 --------MRGSHHHHHHGS..GK.....MD.....A.EF.T.....FA.....
EngBF_L1_F11_v1 .....MD.....A.EF.T.....FA.....
F11, v2 -----.RGSHHHHHHGSDLGKK.LE..MD.QDDE
EngBF_L1_F11_v2 .....MD.....
1580 1590 1600 1610 1620 1630 1640
EngBF_L1_G10 VEVLLKTGADVNAEDMMGFTPLHLAAAWGHLEIVEVLLKHGADVNAQDNQGVTPLHLAAYEGHLEFVEVL
E4, v1 .....Q.VT.T.....V...D.....A.....WH.E..FD..HR.NEDIA...
EngBF_L1_E4_v1 .....Q.VT.T.....V...D.....A.....WH.E.....HR.....
E4, v2 .RI.MAN.....R..Y.Q.....FR.....T.....VT.T.....AV...DI....
EngBF_L1_E4_v2 .....R..Y.Q.....FR.....T.....VT.T.....AV...DI....
F11, v1 .....D.VL.D.....YF.....D.....HW.W..FD..WW.NEDIA...
EngBF_L1_F11_v1 .....D.VL.D.....YF.....D.....HW.W.....WW.....
F11, v2 .RI.MAN.....A.EF.T.....FA.....T.....D.VL.D.....F....I....
EngBF_L1_F11_v2 .....A.EF.T.....FA.....T.....D.VL.D.....F....I....
1650 1660 1670 1680 1690
EngBF_L1_G10 LKHGADVNAQDCFGKTPFDLAIDNGNEDIAEVLQKAAKLGSLEVLFQ-
E4, v1 Q.AAKLNDYK.DDD.----------
EngBF_L1_E4_v1 .....------
E4, v2 ..A.....WH.E.....AHR.....NDYKDDDDK
EngBF_L1_E4_v2 ..A.....H.E.....AHR.....ND-------
F11, v1 Q.AAKLNDYK.DDD.----------
EngBF_L1_F11_v1 .....------
F11, v2 ..D.....HW.W.....AWW.....NDYKDDDDK
EngBF_L1_F11_v2 ..D.....W.W.....AWW.....ND-------

Figure 2

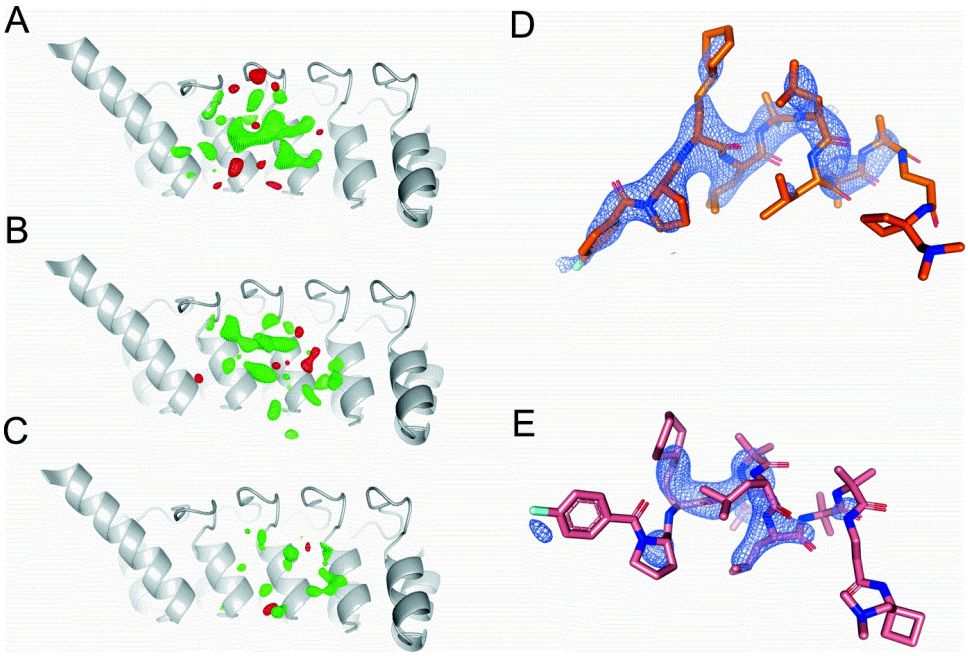

Figure 3

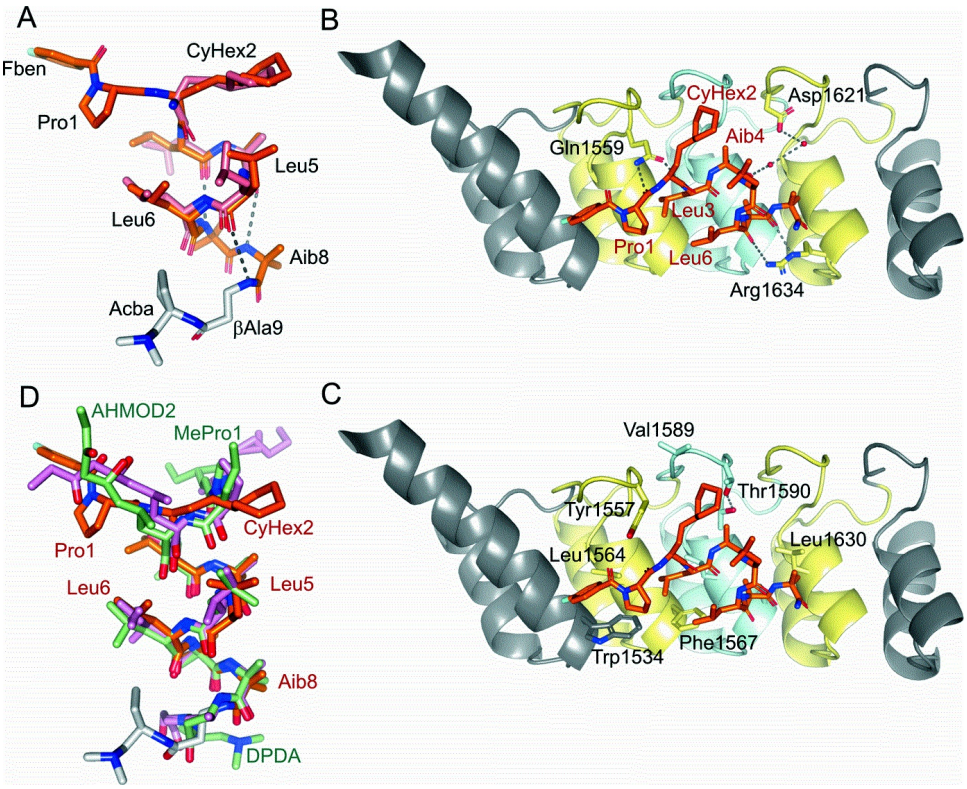
A
Fben
CyHex2
Pro1
Leu5
Leu6
Aib8
Acba
βAla9
B
CyHex2
Asp1621
Aib4
Gln1559
Leu3
Pro1
Leu6
Arg1634
D
AHMOD2
MePro1
CyHex2
Pro1
Leu6
Leu5
Aib8
DPDA
C
Val1589
Thr1590
Tyr1557
Leu1630
Leu1564
Phe1567
Trp1534

Figure 4